

Reexamined lifetimes of the low-lying states of ^{86}Zr by recoil distance differential decay measurements

D. Bucurescu¹, C. Mihai¹, C. Costache¹, R. E. Mihai¹, N. Mărginean¹, S. Kisiov¹, N. Florea¹, G. Căta-Danil², I. Căta-Danil¹, R. Lică¹, R. Mărginean¹, A. Negret¹, C. R. Niță¹, S. Pascu¹, L. Stroe¹, G. Suliman¹, R. Șuvăilă¹ and C. A. Ur³

¹*H. Hulubei National Institute of Physics and Nuclear Engineering, Bucharest, Romania*

²*Physics Department, University "Politehnica," Bucharest, Romania*

³*ELI-NP, Bucharest-Măgurele, Romania*



(Received 19 June 2020; accepted 10 August 2020; published 31 August 2020)

The ^{86}Zr nucleus, which has a low-lying level scheme characteristic of a transitional nucleus, presents, according to the existing electromagnetic transition data, a subunitary $B_{4/2} = B(E2, 4_1^+ \rightarrow 2_1^+)/B(E2, 2_1^+ \rightarrow 0_1^+)$ ratio, which is anomalously low for a nonmagic nucleus, as it is outside the range of the traditional collective models values. In order to check this anomaly, we performed new measurements of the lifetimes of its low-lying states, with the γ -ray coincident recoil distance Doppler shift method, using the ROSPHERE detector array. New lifetimes were determined for the positive-parity yrast states up to the 10^+ one, and for the 8_2^+ , 5_1^- , and 7_1^- states. The newly determined values of the $B(E2)$ values for the 2_1^+ and 4_1^+ states characterize a nucleus with a moderate quadrupole deformation and are well described by the interacting boson model. The ratio $B_{4/2} = 1.38(22)$ is no longer anomalous. The low $B(E2)$ value of the 6_1^+ state indicates a noncollective structure.

DOI: [10.1103/PhysRevC.102.024336](https://doi.org/10.1103/PhysRevC.102.024336)

I. INTRODUCTION

The motivation of the present experimental reinvestigation of the lifetimes of low-lying states in ^{86}Zr is the apparently unusual behavior of the presently known $B(E2)$ values of the lowest states from its ground-state band [1]. With 46 neutrons, ^{86}Zr makes the transition from the spherical Zr isotopes (with $N = 48, 50$), described by multiparticle shell model configurations, to deformed ones (below $N = 44$). Its low-lying level scheme shows the behavior of a slightly anharmonic vibrator (up to spin $6\hbar$). On the other hand, its presently adopted values [1] lead to a ratio $B_{4/2} = B(E2; 4_1^+ \rightarrow 2_1^+)/B(E2; 2_1^+ \rightarrow 0_1^+)$ of 0.67(32). This subunitary ratio, for a nucleus not so close to the 28 and 50 magic numbers, is rather unusual, as it is far from any of the values expected from different collective models (which are between 1 and 2). In some similar cases of other nuclei considered as anomalous from this point of view [2] (e.g., ^{134}Ce [3], ^{98}Ru [4], ^{180}Pt [5]), the reinvestigation of the lifetime measurements corrected this ratio from values $B_{4/2} < 1$ to $B_{4/2} > 1$.

A critical look at the articles reporting lifetimes for the low-lying states in ^{86}Zr shows that those measurements may contain flaws. The present ENSDF values for the low-lying states [1] were adopted on the basis of two measurements. The first is based on recoil-distance Doppler shift (RDDS) measurements performed in the fusion-evaporation reaction $^{73}\text{Ge}(^{16}\text{O}, 3n\gamma)^{86}\text{Zr}$ [6]. It was a noncoincident (singles) measurement, with just one Ge(Li) detector. The lifetimes of the states from the ground-state band up to 8^+ were extracted by simultaneously fitting the decay curves of all four excited

states measured as a function of distance with a large number of parameters (lifetimes, the true zero distance, and some normalization constants). The side feeding times were neglected in this analysis. The level and decay scheme used in the analysis (from Ref. [7]) did not contain one important transition that was added later: the 1006-keV transition above the 3424-keV 7^- level (see the discussion below), which, due to the relatively weak energy resolution of the used Ge(Li) detector, was not even distinguished from the 1003-keV decay transition of the 6^+ level. The second experiment [8] was a similar one, with the RDDS in two fusion-evaporation reactions with a ^{32}S beam. Being also a singles measurement, it provided results that were rather similar with those of the older experiment [6]. For both these experiments, there are reasons to suspect that the reported values are flawed due to the complexity of the spectra and of the feeding of the levels in the reaction, which could not accurately be taken into account into a singles RDDS experiment.

Subsequent experiments also measured lifetimes in this nucleus with the RDDS method and/or Doppler shift attenuation method (DSAM), but only for higher lying levels [9–11].

In the present work, we report RDDS measurements with the same reaction as that used in the previous experiment [6] but performed with a modern detector array and plunger apparatus [12], which allowed the determination of the lifetimes in the γ - γ coincident mode, with the differential decay curve method [14]. In this way, more accurate lifetimes could be determined which eliminate the puzzle of an anomalously low $B_{4/2}$ value.

II. EXPERIMENT, ANALYSIS, AND RESULTS

A. Experiment

The experiment was performed at the 9-MV Tandem Van de Graaff accelerator of our institute, with a ^{16}O beam of 57-MeV energy. The target consisted of 0.4-mg/cm^2 ^{73}Ge (95.6% isotopically enriched) deposited on a 3-mg/cm^2 stretched Au foil. The ion beam current on the beam was kept below 4 pA. The stopper was a 5-mg/cm^2 stretched Au foil. Both the ROSPHERE detector array and plunger device are described in Ref. [12]. ROSPHERE was used in one of its configurations, with 15 HPGe detectors with BGO shields and 9 $\text{LaBr}_3(\text{Ce})$ detectors. The Ge detectors were arranged into three rings: five at 90° (the ring 90), five in the forward (F) ring at 37° , and five in the backward (B) ring at 143° . Double $\gamma\text{-}\gamma$ (Ge-Ge) and triple $\gamma\text{-}\gamma\text{-}\gamma$ (Ge- LaBr_3 - LaBr_3) coincidences were registered event by event for subsequent processing. Spectra were measured at ten distances of 10, 20, 30, 50, 70, 110, 150, 200, 250, and $300\ \mu\text{m}$ with respect to the “zero” distance inferred from the extrapolation of the capacity versus distance calibration curve. The acquisition of each spectrum was made for at least 24 h. The velocity of the recoiling nuclei was $v/c = 0.0123$ and therefore the shifted peaks in the F and B detectors had energies practically equal to $(1 \pm 0.01)E_\gamma$, respectively.

B. Data analysis

For the differential decay curve method (DDCM) analysis, the data recorded by the HPGe detectors were sorted into seven $\gamma\text{-}\gamma$ coincidence matrices at each distance: 90-90 (between the detectors of the 90° ring), 90-F (between the detectors of the 90 and F rings), 90-B (90 and B), FF (between the detectors of the F ring), BB (between the detectors of the B ring), FB (between the detectors of the B and F rings), and its transposed BF (the notation BF denotes, e.g., that on the two axes of the matrix are the projection spectra of the detectors from the respective rings). While the matrices without 90° detectors (FF, BB, FB, and BF) were directly used in the DDCM analysis, those having the 90° detectors on at least one axis were useful to more clearly examine the cleanliness of the gates involved in the DDCM analysis, which is of interest to find and avoid unwanted superpositions with other γ rays from the dense total spectra.

Figure 1 shows a partial level scheme of ^{86}Zr [1], which is useful to follow the way the DDCM analysis was performed. In this method, a transition from the level of interest is examined in a gate on the shifted component (S component) of a transition above the level. This transition may directly feed the level, or indirectly, through an intermediate transition (e.g., 752 keV gated by the S peak of 915 keV or the S peak of the 1003 keV, respectively). One must take care that the S peak of the gating transition does not overlap with another transition also involved in coincidence relationship with the studied transition of the level—in the example above, the forward S peak of 915 keV overlaps with the U peak (U denotes unshifted) of the 925-keV transition which is also coincident with 752 keV (Fig. 1), and therefore this gating on the F spectra cannot be used.

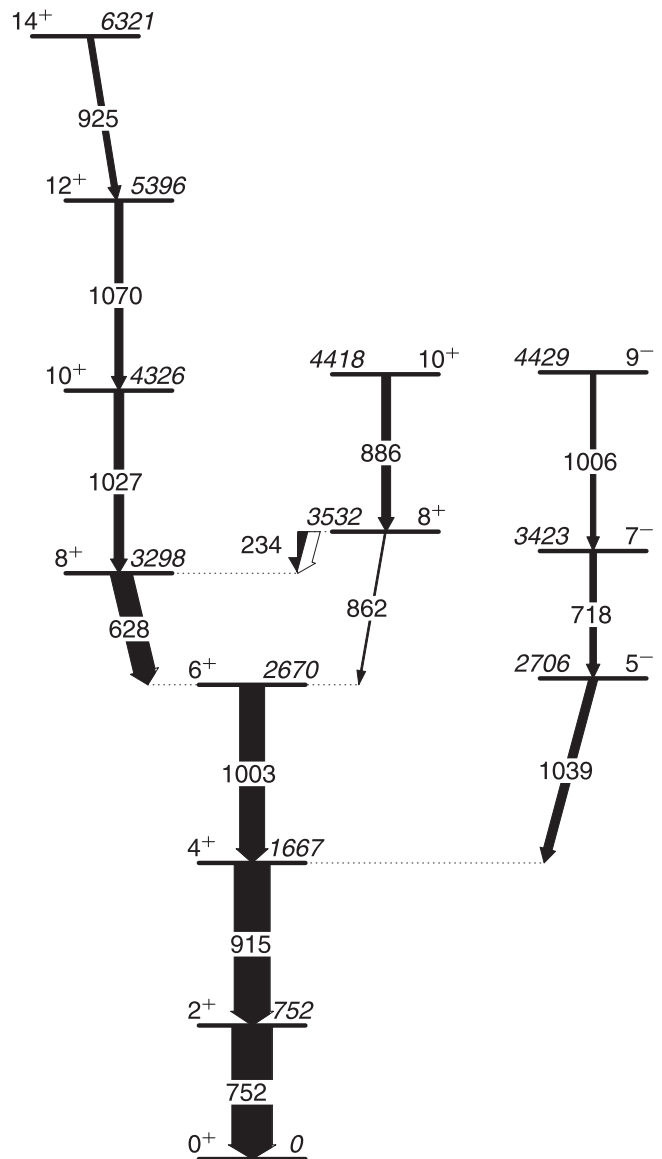


FIG. 1. Partial level scheme of ^{86}Zr [1], relevant for the present measurements. Illustrative γ -ray intensities shown by the arrow thicknesses were taken from Ref. [13].

For each investigated transition, spectra gated on the S peak of the feeding transition were generated at each distance. In general, if the S-peak gates were clean in both F and B rings, four spectra were generated from the four matrices specified above. They were added two by two to get two spectra in which the S peak of the studied transition is backward (B) or forward (F) shifted, respectively. From each of these spectra, the intensities of the S and U components of the studied transition were determined. At the larger distances, where the U component is usually small and cannot be accurately determined or even clearly seen, we added the four spectra, such as the unshifted peak became more visible, and analyzed the U peak and the two S peaks. The determined intensities of the shifted and unshifted peaks were finally all added and normalized at each distance. For normalization, we used the sum of the intensities of the 752- and 915-keV transitions

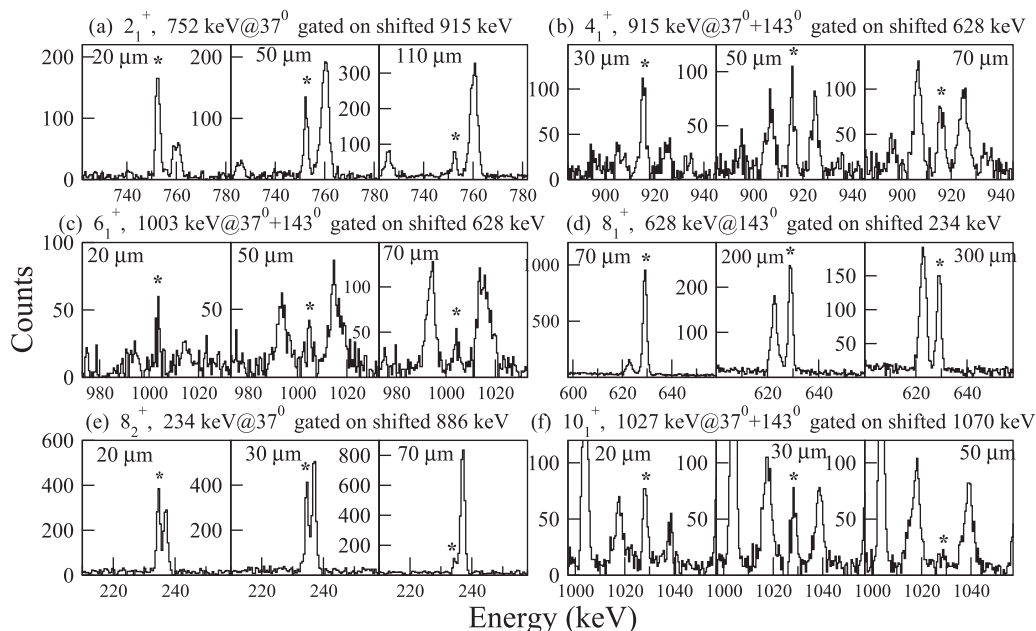


FIG. 2. Examples of the evolution of gated spectra as a function of distance, for the positive-parity states measured in this work. The stopped peak of the followed transition is always in the center of the graph and is marked with an asterisk.

from the projection axis of the 90:90 matrix. The normalized intensities as a function of distance were analyzed with the DDCM method in order to extract the lifetime of the state under consideration.

Figure 2 shows different examples of spectra with the level decay transitions from the positive-parity states measured in this experiment, gated on the shifted component of a transition from above. In each case, three distances were chosen such as to illustrate how the shifted and unshifted components completely change their relative intensities over a certain range of distances. The spectra were very clean and the peaks of interest could be accurately processed.

Figure 2(a) shows the $2_1^+ \rightarrow 0_1^+$ transition seen in the F detectors, by gating on the shifted peak of the directly feeding 915-keV transition in the B detectors. Figure 2(b) is an example of indirect gating: 915-keV, $4_1^+ \rightarrow 2_1^+$, gated by the S peak of the 628-keV transition which feeds the 4_1^+ level through the 1003-keV transition, as seen in both F and B detectors taken together. The labels and aspects of Figs. 2(c) to 2(f) are self-explanatory. The last graph of this figure, Fig. 2(f), illustrates how the total spectrum (resulted from the addition of all four spectra as explained above) is useful to evaluate the small unshifted peak of the 1027-keV transition at the largest distance where it could still be observed and integrated (in the individual spectra, this peak was practically unobservable). Each of these transitions will be discussed in detail later.

Figure 3 is similar to Fig. 2, showing the evolution of the gated spectra with the distance, for the two negative-parity states measured in this experiment.

C. Lifetime analysis and results

The decay curves (variation of the intensities of the shifted and unshifted components of a gated transition as a function of

distance) obtained as described above were analyzed with the DDCM procedure [14]. In this procedure, for each distance x one determines a lifetime through the formula:

$$\tau = \frac{\{B_S, A_U\}(x)}{d\{B_S, A_S\}(x)/dx v}, \quad (1)$$

where the quantities in brackets denote the areas of the shifted (S) peak and unshifted (U) peaks, respectively, of transition A gated by the S peak of the feeding transition B.

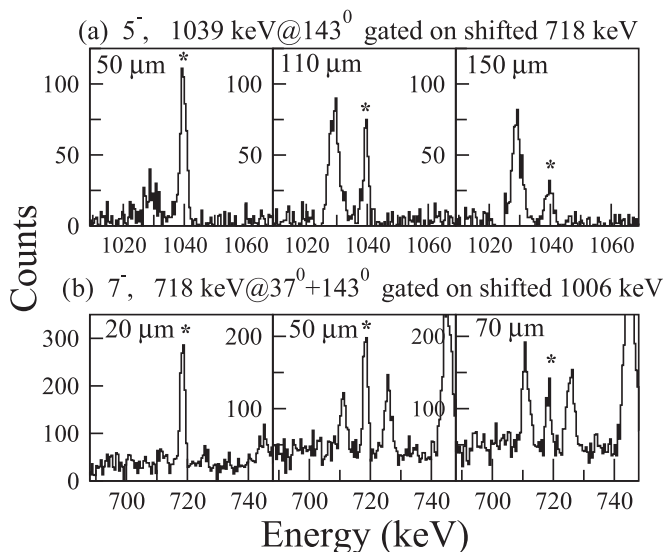


FIG. 3. Same as Fig. 2, but for negative-parity states.

For the case of an indirect gating (gate on transition C which feeds A through B), the formula is

$$\tau = \frac{\{C_S, A_U\}(x) - \alpha \{C_S, B_U\}(x) \frac{1}{v}}{d\{C_S, A_S\}(x)/dx}, \quad (2)$$

where

$$\alpha = \frac{\{C_S, A_U\}(x) + \{C_S, A_S\}(x)}{\{C_S, B_U\}(x) + \{C_S, B_S\}(x)}.$$

The intensity of the S peak of the observed transition, as a function of distance, is fitted by a number of smoothly joined second-degree polynomials, which are then used to calculate the derivatives from Eqs. (1) or (2). We usually employed two polynomials, with the exception of the 752-keV transition observed in the 915-keV gate, where we chose three polynomials. Both the S and U components of the transition as a function of distance x were simultaneously fitted to provide a lifetime τ for each of the distance points considered in the fit. The adopted lifetime is the weighted average of these values.

Figure 4 displays the lifetime analysis for the 2_1^+ , 4_1^+ , and 6_1^+ states.

1. The 2_1^+ state

Figure 4(a) shows two independent determinations of the lifetime. The first one is from the direct gating on the transition above the state, 915 keV ($4^+ \rightarrow 2^+$). As mentioned earlier, only the gate on the backward-shifted peak of 915 keV could be used, because the forward-shifted peak mixes with the shifted component of the 925-keV, $14^+ \rightarrow 12^+$ transition (see Fig. 1). The second determination is from indirect feeding, by gating on the 1039-keV, $5^- \rightarrow 4^+$ transition. In this case, only gating on the forward-shifted peak was useful because in the backward direction the shifted peak of 1039-keV transition partly overlaps with the stopped peak of the 1027-keV, $10^+ \rightarrow 8^+$ transition.

2. The 4_1^+ state

The 915-keV decay transition of this level was observed [Fig. 4(b)] in three independent ways: a direct gating and two indirect ones. The direct gating was with the 1039-keV transition. A direct gating with the transition 1003 keV, $6^+ \rightarrow 4^+$ was impossible, because this energy is too close to that of the 1006-keV, $9^- \rightarrow 7^-$ transition and practically one could not get rid of the contribution of the latter. The second determination is with an indirect gating on the 628-keV ($8^+ \rightarrow 6^+$) transition. The third one is again a case of indirect feeding, with the 718-keV ($7^- \rightarrow 5^-$) transition. Here only gating on the forward-shifted peak of 718 keV was useful. The reason was that in the spectra there is a γ ray at an energy of 710 keV which is coincident with a γ ray of 914.3 keV (apparently not in ^{86}Zr), and its stopped peak energy overlaps with that of the backward-shifted peak of 718 keV. The values obtained from the three independent determinations agree with each other reasonably well.

3. The 6_1^+ state

Figure 4(c) shows a determination from direct gating on the 628 keV ($8^+ \rightarrow 6^+$) transition. The fit of data obtained with

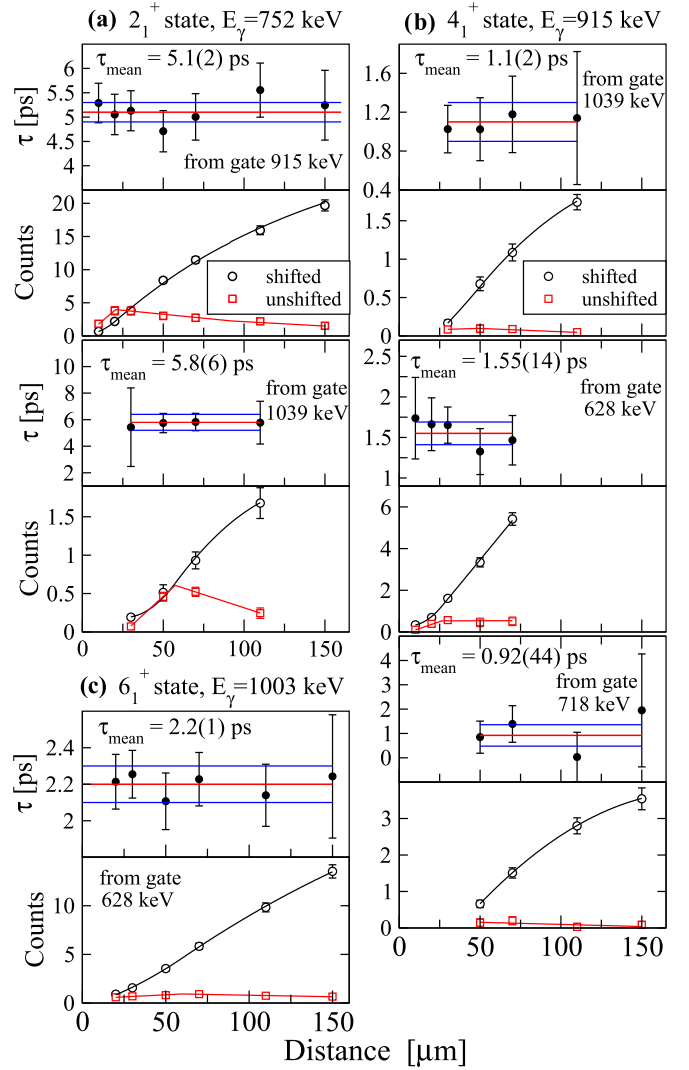


FIG. 4. Results of the DDCM analysis for the determination of the lifetimes of the first three positive-parity yrast states. In each case, the gate was set on the shifted component of the indicated γ ray, and the fit was made to both shifted and unshifted components of the investigated transition. In the case of the indirect gates, the intensity of the shifted component from the graph is that corrected with the α factor according to Eq. (2).

an indirect gating on the 1027-keV transition gave a value of 3.3(14) ps, which confirms the value of 2.2 ps obtained by the direct 628-keV gate. However, because of the large error, this latter value does not significantly contribute to the result obtained by a weighted average of the two values.

Figure 5 shows the analysis for the 8_1^+ state. Two direct gatings were used, one on the 234-keV, $8_2^+ \rightarrow 8_1^+$ transition, and the other one on the 1027-keV, $10_1^+ \rightarrow 8_1^+$ transition. This transition has a relatively long lifetime; however, it was shown that deorientation has no effect in the case of direct gating from above [15].

Figure 6 displays the lifetime analysis of other four states: 8_2^+ , 10_1^+ , 5_1^- , and 7_1^- . In each case, a direct gating was used. For the 7_1^- state, a gate on the transition 1006 keV above this

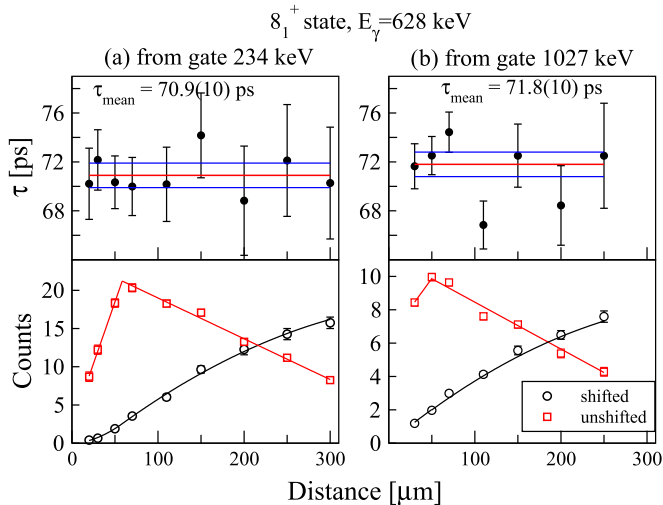


FIG. 5. Same as Fig. 4; the DDCM analysis for the determination of the lifetime of the 8_1^+ state.

state was used. This was a wide gate, with contribution also from the 1003-keV transition, but, since this transition is not coincident with 718 keV, it had no influence on the result.

4. Fast-timing lifetime determination for the 8_1^+ state

The lifetime of this state, of 70 ps, is also in the domain of the fast-timing method [16]. Because our data contained

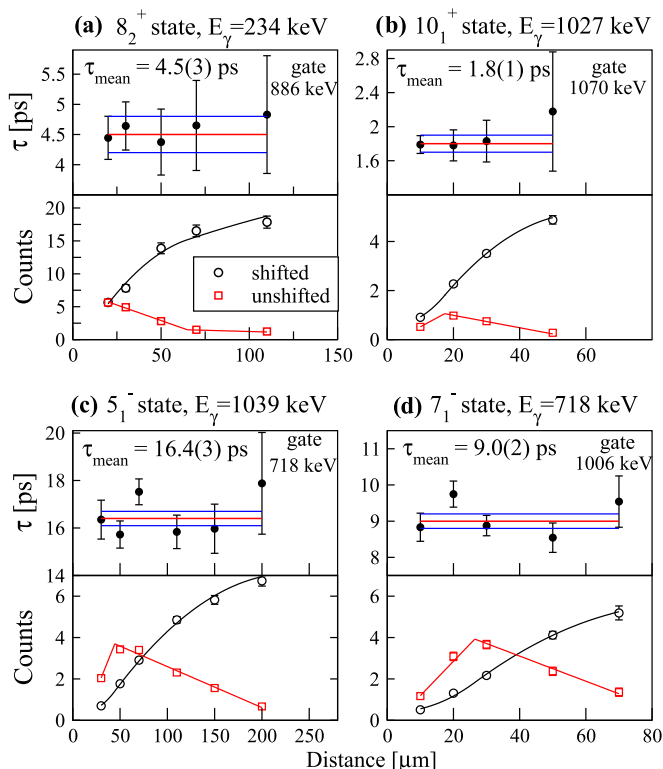


FIG. 6. Same as Fig. 4 but for the 8_2^+ , 10_1^+ states, and the negative-parity states 5_1^- and 7_1^- .

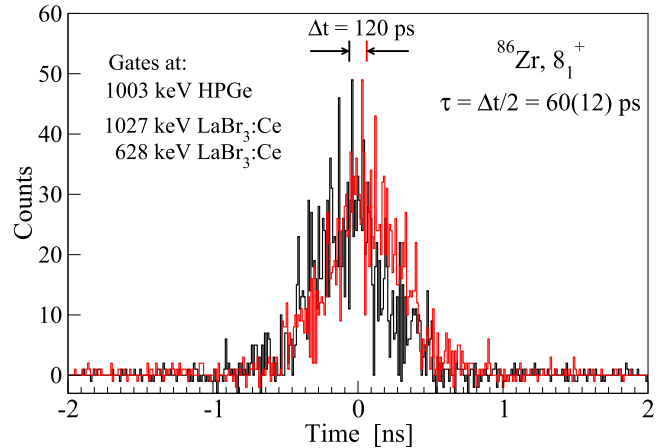


FIG. 7. Determination of the lifetime of the 8_1^+ level with the fast-timing method (centroid version) [16]. The two time spectra were obtained in the following way: one with the 1027-keV transition as a start and the 628-keV one as a stop, and the second one with the 628-keV one as start and the 1027-keV one as stop, respectively.

the events from the the fast $\text{LaBr}_3(\text{Ce})$ detectors, we made an attempt to determine this lifetime by this method too.

The method implies sorting triple- γ coincidences (Ge- LaBr_3 - LaBr_3), between one HPGe detector and two LaBr_3 detectors. With a gate on the high-resolution Ge detector, one can select in the LaBr_3 spectra a cascade of two transitions, feeding and deexciting the level of interest, respectively. From a matrix $\Delta t - E_{\gamma 1} - E_{\gamma 2}$, where Δt is the time difference between events in the two LaBr_3 detectors, one obtains the decay time spectrum of the selected level. A result of this method, in its version in which the lifetime is deduced from the shift of the centroid of the time spectrum when the two transitions are used, each one both as a start and as a stop in the time spectrum, is shown in Fig. 7. The cascade of the 1027- and 628-keV γ rays in LaBr_3 was selected by gating on the 1003-keV transition in the HPGe detectors. We have included in the data sorting all HPGe detectors and gated only on the unshifted component of the 1003-keV transition. One could not combine more HPGe- LaBr_3 gates because in this experiment, focused on the RDDS measurement, we have not performed a calibration with radioactive sources in order to determine a precise correction for the time walk of the fast detector signals with the energy [16]. Therefore, we have used such a correction from one of the previous experiments with ROSPHERE in the same configuration. The uncertainty of the determined lifetime (Fig. 7) is rather large because the statistic is not high. Nevertheless, the value of the lifetime is consistent with that determined from the RDDS experiment.

The results from the present lifetime determinations are collected in Table I, where they are also compared to the previously known values. For the first four states, the ENSDF adopted values are based on Refs. [6,8]. From Figs. 4 to 6 and Table I, one can see that in our experiment, when more lifetimes were determined for one level by different gating conditions, they agree rather well. The most significant differences from the previous values [1] has been found for the first three states from the ground-state band. A particularity

TABLE I. Results for the lifetimes measured in the present experiment. The third column gives the γ -ray transition for which the decay curves (variation of the shifted and unshifted components, respectively) were measured from spectra gated on the shifted component of the transition shown in the fifth column (except for the weak 862-keV, 15% branch of the 3532-keV state). The lifetime values from column 8 labeled as “present mean τ ” are the weighted averages of the results of the present independent determinations given in column 7, and they were used to calculate the B values given in the last two columns. See also Fig. 1.

E_x (keV)	J^π	E_γ (keV)	Final state	Gate (keV)	τ [ENSDF] (ps)	τ [this work] (ps)	Present mean τ (ps)	$B(E2; J \rightarrow J - 2)$ (W.u.)	$B(X1)$ (W.u.)
752	2_1^+	752	0_1^+	915 1039	10.8(20)	5.1(2) 5.8(6)	5.2(3)	29.0(17)	
1667	4_1^+	915	2_1^+	1039 628 718	7.8(35)	1.1(2) 1.55(14) 0.92(44)	1.4(2)	40(6)	
2670	6_1^+	1003	4_1^+	628	12.3(49)	2.2(1)	2.2(1)	16.5(11)	
3298	8_1^+	628	6_1^+	234 1027 FT ^a	66.4 (87)	70.9(10) 71.8(10) 60(12)	71.3(7)	5.18(6)	
3532	8_2^+	234 862	8_1^+ 6_1^+	886	4.8(10)	4.5(3)	4.5(3)	<290 ^b 2.3(6)	>0.42 (M1)
4326	10_1^+	1027	8_1^+	1070	3.1(6)	1.8(1)	1.8(1)	17.2(10)	
2706	5_1^-	1039	4_1^+	718	9.7(17)	16.4(3)	16.4(3)		2.71×10^{-5} (E1)
3423	7_1^-	718	5_1^-	1006	9.8(22)	9.0(2)	9.0(2)	21.3(4)	

^aObtained with the fast-timing method (see text).

^bM1(+E2), $\delta < 0.17$ [1].

of our reaction is that these states are strongly fed by the relatively long-living 8_1^+ state (see Fig. 1). This allowed us to investigate short lifetimes at relatively long distances, as we have also checked by simulation calculations. As one can see in the spectra of Figs. 2 and 3, the 4_1^+ and 6_1^+ states show significant changes of the relative intensity of the S and U components of their decay transitions over a relatively broad range of distances (from 20 to 70 or even 150 μm), and the analysis of their decay curves (Fig. 4) results in lifetimes with values in the range ≈ 1 to 2 ps. As both Eqs. (1) and (2) show, the shape of the (corrected) unshifted component as a function of distance is given by the derivative of the shifted component curve, while its magnitude is also proportional to the lifetime of the state.

III. DISCUSSION AND CONCLUSION

The structure of the ^{86}Zr nucleus was mainly discussed in the literature in connection with its higher spin states (above spin $8\hbar$). Its low-lying structure remained rather puzzling until now. Reference [17] discussed the evolution of the low-lying levels in the Sr and Zr isotones with $N = 40$ to 46 within the frame of the interacting boson model-1 (IBM-1) [18]. The two chains are rather similar, and were described with the same model parameters. The yrast structure of the nuclei with $N = 44$ and $N = 46$ were reasonably well described up to spin 6 as that of vibrators with some anharmonicity. At $N = 46$, both Sr and Zr present a backbending at spin 8, which was interpreted as due to the breaking of a pair of nucleons from the high-spin orbital $g_{9/2}$ (see, e.g., Ref. [19]). The decreasing pattern of the (old) $B(E2)$ values of the lowest states from the ground state band of the $N = 46$ nuclei was not understood, and was tentatively attributed to a lower collectivity of these states

(perhaps due to admixture of collective and quasiparticle degrees of freedom, which is important around $N = 46$).

A first attempt to understand the $B(E2)$ evolution with spin, at both low and higher spins, was made in Ref. [10], on the basis of an extension of the IBM-1 model to higher spins: IBM-1 with two broken nucleon pairs [20]. This is a hybrid model, which combines the collective quadrupole degrees of freedom with single-particle ones by explicitly considering two or four $g_{9/2}$ nucleons above the first backbending. It can mix 0, 2, and 4 quasiparticles which can couple to their respective cores. The results of this model, discussed also in Ref. [21], showed a reasonable agreement with the pattern of the evolution of the $B(E2)$ strengths with spin (up to spins $\approx 20\hbar$). However, the model failed to describe the behavior of the $B(E2)$ values at low spins, where ^{86}Zr was described as a slightly anharmonic vibrator, close to the U(5) symmetry (similarly to Ref. [17]). This situation led to some speculations, as further discussed in Ref. [22]. A pattern of decreasing $B(E2)$'s, as seen in the old data at low spins, may be due, within the framework of collective models, to shape changes or band crossings. This scenario was, however, rather implausible, because both the level spacings and the g factors of the 8^+ state (in ^{84}Sr [23]) showed that the 0-qp vibrational state and the 2-qp 8^+ state had rather pure, unmixed configurations. Therefore, another scenario was speculated: The possible truncation of the shell model space. In the IBM-1 description, the number of active particles, which determines the number of bosons, was counted with respect to the classical magic numbers Z , $N = 28, 50$, and therefore ^{86}Zr has $N = 7$ bosons. If in the U(5) limit we count now the numbers assuming that we have a subshell closure at $Z, N = 40$, then $N = 2$ for ^{86}Zr and $N = 3$ for ^{84}Sr . In this case, one gets a better description of the low-lying levels decay pattern. For $N = 2$, the calculated $B(E2)$ value for the $4^+ \rightarrow 2^+$ transition is almost equal to

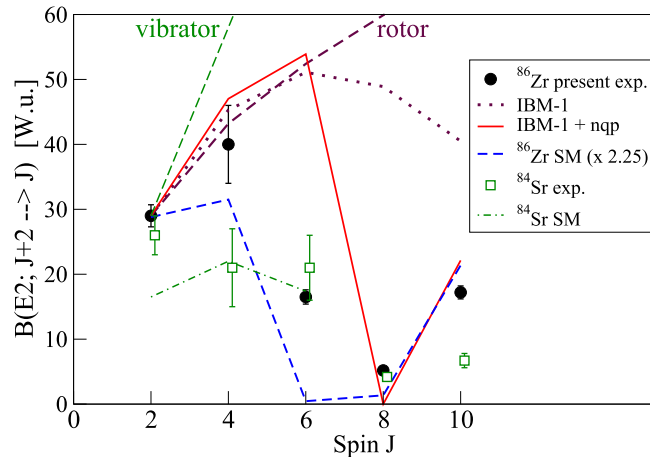


FIG. 8. Evolution of the $B(E2)$ values for the lowest yrast positive-parity states, from the present determinations in ^{86}Zr , and from Ref. [24] in ^{84}Sr , compared to predictions of different models (see also text): IBM-1 and IBM-1 with broken pairs [21]; and shell-model calculations for ^{86}Zr [25] (note the change of scale of these values), and for ^{84}Sr [26], respectively.

that of the $2^+ \rightarrow 0^+$ one, and that for $6^+ \rightarrow 4^+$ is zero as two bosons cannot generate a spin 6 [22]. Although in this way one qualitatively described the observed experimental behavior [decreasing $B(E2)$'s], it was puzzling why one should truncate so much of the shell model space at low spins, while at higher spins the truncation with respect to the classical magic numbers had to be restored.

The present data on the low-lying states have partially solved this puzzle. Figure 8 shows the $B(E2)$ values measured in this work, compared to predictions of several models. In the IBM-1 calculations, we have used the parameters of Refs. [21,22], which are very close to those proposed in Ref. [17]. With an effective boson charge of 0.08 eb, as proposed in [17], one calculates a $B(E2; 2_1^+ \rightarrow 0_1^+)$ value that is practically equal to the one found in the present experiment. The values of the calculation with the IBM-1 with broken pairs [21,22] were renormalized in this figure to the new experimental $B(E2; 2_1^+ \rightarrow 0_1^+)$ value. One can see that both models correctly predict the observed increase from spin 2 to spin 4, and the IBM-1 with broken pairs also describes the strong decrease for the value of the two-qp state of spin 8. On the other hand, there is still severe disagreement with the value of the 6^+ state. Its experimental $B(E2)$ value is much lower, suggesting less collectivity of this state.

Figure 8 also shows the experimental $B(E2)$ values in the isotonic nucleus ^{84}Sr [24]. They are rather similar with those determined in this work for ^{86}Zr , except for the $B(E2; 4_1^+ \rightarrow 2_1^+)$ value, which is lower than the $B(E2; 2_1^+ \rightarrow 0_1^+)$ one. According to these values, the $B_{4/2}$ ratio of ^{84}Sr is 0.81(25), practically outside the range predicted by different collective models. The situation may be somewhat similar to that encountered until now for ^{86}Zr .

The $B(E2)$ value of the 6_1^+ state in ^{88}Mo is also lower than that of the 4_1^+ state [27], and therefore this is a systematic feature in the $N = 46$ isotones, indicating that in the structure

of the states of spin higher than 4 in these nuclei there is a decrease of collectivity. The causes of this change may be found by considering the microscopic structure of these states. Considerations along these lines were made in Ref. [28]. A comparison between ^{88}Zr and ^{86}Zr shows that, while the 8^+ , and to some extent, the 6^+ states remain relatively constant in energy, the 4^+ and 2^+ states are more compressed in energy in ^{86}Zr . This energy compression may be due to a deformation setting in, while the higher states may be associated with domination of the neutron excitations of the type $g_{9/2}^{-4}$ with seniority $\nu = 2$.

A more precise answer was given by subsequent shell model (SM) calculations for nuclei from this mass region. Thus, a general study of the multiparticle-hole states in nuclei of mass $A \approx 90$ and $N < 50$ was made in Ref. [29] with SM calculation in a space truncated to $1g_{9/2}, 2p_{1/2}$ for both protons and neutrons, with both empirical and schematic two-body matrix elements. These calculations tested the purity of seniority in these nuclei, the effect of enlargement of the space (by adding the orbitals $1f_{5/2}$ and $2p_{3/2}$), as well as the onset of quadrupole collectivity near $N = 46$. The application of this type of calculations to the $N = 46$ isotones was made in Ref. [25]. The calculations showed that this space truncation describes reasonably well the higher spin members of the $[\pi^2(g_{9/2}) \times \nu^{-4}(g_{9/2})]$ configurations, but it is too severe for the low-spin states. The spacings of the states below spin 8 are not well described, as they show a typical $(g_{9/2})^2$ spectrum, in contrast to the almost equidistant experimental one. The SM predictions for the $B(E2)$ values show only a qualitative agreement in this region. These predictions for ^{86}Zr are included in Fig. 8; they are too small in absolute value (note the renormalization by a factor of 2.25 in the figure) and largely accentuate the minimum for the $B(E2)$ transitions of the 8^+ and 6^+ states.

More extended SM calculations were performed for the nuclei ^{88}Sr , ^{86}Sr , and ^{84}Sr [26] in a truncated $(2p_{3/2}, 1f_{5/2}, 2p_{1/2}, 1g_{9/2})$ model space with the empirical JUN45 residual interaction. While in ^{86}Sr the 6_1^+ and 8_1^+ states have a relatively pure seniority 2 character (all nucleons coupled in pairs, protons in the ground state of spin 0, and the two neutron holes from the $1g_{9/2}$ orbital forming the spins 6 and 8, respectively), in ^{84}Sr (the isotone of ^{86}Zr) these states have an increased configuration mixing, with important contributions from proton excitations from $f_{5/2}$ into the $p_{1/2}$ and $g_{9/2}$ orbitals, indicating an increased collectivity. Among the lowest yrast states ($2^+, 4^+, 6^+$), the 6_1^+ state has the largest $[\nu g_{9/2}^{-4}]6^+$ component. The $B(E2)$ values predicted for the first yrast states are also shown in Fig. 8. While the experimental $B(E2)$ values of the 4_1^+ and 6_1^+ states are well described in absolute value, that of the 2_1^+ state is underestimated by about 40% [26]. Although one cannot draw a conclusion on how similar calculations would describe the situation in the isotone ^{86}Zr , it is interesting to remark that the pattern of the variation of the first three yrast $B(E2)$ values calculated for ^{84}Sr is rather similar to that of the experimental values from our nucleus.

In conclusion, this work presented new, precise measurements of the lifetimes of low-lying, low-spin states in the transitional nucleus ^{86}Zr . The new $B(E2)$ values for this

nucleus give a ratio of $B_{4/2} = 1.38(22)$ which, together with the quadrupole deformation $\beta_2 = 0.21$ (as determined from the $B(E2; 2_1^+ \rightarrow 0_1^+)$ value) shows that at low spins this nucleus is moderately deformed, and is not anomalous, as it was considered until now. The $B(E2)$ values of the transitions from the 2_1^+ and 4_1^+ states are in good agreement with predictions of collective models. On the other hand, the $B(E2)$ value of the 6_1^+ state is lower than these predictions by a factor of about 3, indicating a strong decrease of the

collectivity with increasing spin. A detailed understanding of this phenomenon remains a challenge for more extended, upcoming microscopic model calculations.

ACKNOWLEDGMENTS

We are grateful to the tandem accelerator crew for the excellent quality beam. We acknowledge partial funding by the Romanian project IFA CERN RO/ISOLDE.

-
- [1] A. Negret and B. Singh, *Nucl. Data Sheets* **124**, 1 (2015).
- [2] R. B. Cakirli, R. F. Casten, J. Jolie, and N. Warr, *Phys. Rev. C* **70**, 047302 (2004).
- [3] B. J. Zhu, C. B. Li, X. G. Wu, J. Zhong, Q. M. Chen, Y. Zheng, C. Y. He, W. K. Zhou, L. T. Deng, and G. S. Li, *Phys. Rev. C* **95**, 014308 (2017).
- [4] D. Radeck, V. Werner, G. Ilie, N. Cooper, V. Anagnostatou, T. Ahn, L. Bettermann, R. J. Casperson, R. Chevrier, A. Heinz, J. Jolie, D. McCarthy, M. K. Smith, and E. Williams, *Phys. Rev. C* **85**, 014301 (2012).
- [5] E. Williams, C. Plettner, E. A. McCutchan, H. Levine, N. V. Zamfir, R. B. Cakirli, R. F. Casten, H. Ai, C. W. Beausang, G. Gurdal, A. Heinz, J. Qian, D. A. Meyer, N. Pietralla, and V. Werner, *Phys. Rev. C* **74**, 024302 (2006).
- [6] M. Avrigeanu, V. Avrigeanu, D. Bucurescu, G. Constantinescu, M. Ivaşcu, D. Panteliciă, M. Tănase, and N. V. Zamfir, *J. Phys. G* **4**, 261 (1978).
- [7] G. Korschinek, E. Nolte, H. Hick, K. Miyano, W. Kutschera, and H. Morinaga, *Z. Phys. A* **281**, 409 (1977).
- [8] R. A. Kaye, J. B. Adams, A. Hale, C. Smith, G. Z. Solomon, S. L. Tabor, G. García-Bermúdez, M. A. Cardona, A. Filevich, and L. Szybisz, *Phys. Rev. C* **57**, 2189 (1998).
- [9] E. K. Warburton, C. J. Lister, J. W. Olness, P. E. Haustein, S. K. Saha, D. E. Alburger, J. A. Becker, R. A. Dewberry, and R. A. Naumann, *Phys. Rev. C* **31**, 1211 (1985).
- [10] P. Chowdhury, C. J. Lister, D. Vretenar, C. Winter, V. P. Janzen, H. R. Andrews, D. J. Blumenthal, B. Crowell, T. Drake, P. J. Ennis, A. Galindo-Uribarri, D. Horn, J. K. Johansson, A. Omar, S. Pilotte, D. Prevost, D. Radford, J. C. Waddington, and D. Ward, *Phys. Rev. Lett.* **67**, 2950 (1991).
- [11] M. Wiedeking, S. L. Tabor, F. Cristancho, M. Devlin, J. Döring, C. B. Jackson, G. D. Johns, R. A. Kaye, I. Y. Lee, F. Lerma, A. O. Macchiavelli, M. Naidu, I. Ragnarsson, D. G. Sarantites, and G. Z. Solomon, *Phys. Rev. C* **67**, 034320 (2003).
- [12] D. Bucurescu, I. Căta-Danil, G. Ciocan, C. Costache, D. Deleanu, R. Dima, D. Filipescu, N. Florea, D. G. Ghiţă, T. Glodariu, M. Ivaşcu, R. Lică, N. Mărginean, R. Mărginean, C. Mihai, A. Negret, C. R. Niţă, A. Olăcel, S. Pascu, T. Sava, L. Stroe, A. Şerban, R. Şuvăilă, S. Toma, N. V. Zamfir, G. Căta-Danil, I. Gheorghe, I. O. Mitu, G. Suliman, C. A. Ur, T. Braunroth, A. Dewald, C. Fransen, A. M. Bruce, Z. Podolyák, P. H. Regan, and O. J. Roberts, *Nucl. Instrum. Methods Phys. Res. Res. A* **837**, 1 (2016).
- [13] J. Döring, Y. A. Akovali, C. Baktash, F. E. Durham, C. J. Gross, P. F. Hua, G. D. Johns, M. Korolija, D. R. LaFosse, I. Y. Lee, A. O. Macchiavelli, W. Rathbun, D. G. Sarantites, D. W. Stracener, G. Z. Solomon, S. L. Tabor, A. Vander Molen, A. V. Afanasjev, and I. Ragnarsson, *Phys. Rev. C* **61**, 034310 (2000).
- [14] P. Petkov, D. Tonev, J. Gableske, A. Dewald, T. Klemme, and P. von Brentano, *Nucl. Instrum. Methods Phys. Res. A* **431**, 208 (1999).
- [15] P. Petkov, *Nucl. Instrum. Methods Phys. Res. A* **349**, 289 (1994).
- [16] N. Mărginean, D. L. Balabanski, D. Bucurescu, S. Lalkovski, L. Atanasova, G. Căta-Danil, I. Căta-Danil, J. M. Daugas, D. Deleanu, P. Detistov, G. Deyanova, D. Filipescu, G. Georgiev, D. Ghiţă, K. A. Gladnishi, R. Lozeva, T. Glodariu I, N. Ivaşcu, S. Kisiov, C. Mihai, R. Mărginean, A. Negret, S. Pascu, D. Radulov, T. Sava, L. Stroe, G. Suliman, and N. V. Zamfir, *Eur. Phys. J. A* **46**, 329 (2010).
- [17] D. Bucurescu, G. Căta, D. Cutoiu, G. Constantinescu, M. Ivaşcu, and N. V. Zamfir, *Nucl. Phys. A* **401**, 22 (1983).
- [18] A. Arima and F. Iachello, *Ann. Phys. (NY)* **99**, 253 (1976); **111**, 201 (1978); **123**, 468 (1979).
- [19] C. A. Fields and F. W. N. de Boer, *Z. Phys. A* **311**, 127 (1983).
- [20] D. Vretenar, V. Paar, G. Bonsignori, and M. Savoia, *Phys. Rev. C* **42**, 993 (1990); D. Vretenar, V. Paar, M. Savoia, and G. Bonsignori, *ibid.* **44**, 223 (1991).
- [21] A. A. Chishti, P. Chowdhury, D. J. Blumenthal, P. J. Ennis, C. J. Lister, C. Winter, D. Vretenar, G. Bonsignori, and M. Savoia, *Phys. Rev. C* **48**, 2607 (1993).
- [22] C. J. Lister, P. Chowdhury, and D. Vretenar, *Nucl. Phys. A* **557**, 361c (1993).
- [23] A. I. Kucharska, J. Billowes, and C. J. Lister, *J. Phys. G* **15**, 1039 (1989).
- [24] B. Singh, A. Negret, and K. Zuber, *Nucl. Data Sheets* **110**, 2815 (2009).
- [25] E. Galindo, A. Jungclaus, and K. P. Lieb, *Eur. Phys. J. A* **9**, 439 (2000).
- [26] H. Duckwitz, P. Petkov, T. Thomas, T. Ahn, A. Blazhev, N. Cooper, C. Fransen, M. Hinton, G. Ilie, J. Jolie, and V. Werner, *Nucl. Phys. A* **965**, 13 (2017).
- [27] E. A. McCutchan and A. A. Sonzogni, *Nucl. Data Sheets* **115**, 135 (2014).
- [28] J. E. Kitching, P. A. Batay-Csorba, C. A. Fields, R. A. Ristinen, and B. L. Smith, *Nucl. Phys. A* **302**, 159 (1978).
- [29] D. Rudolph, K. R. Lieb, and H. Grawe, *Nucl. Phys. A* **597**, 298 (1996).